



Weldability of neutron irradiated austenitic stainless steels

Kyoichi Asano ^{a,*}, Seiji Nishimura ^b, Yoshiaki Saito ^b, Hiroshi Sakamoto ^c,
Yuji Yamada ^d, Takahiko Kato ^e, Tsuneyuki Hashimoto ^f

^a *Materials Engineering Group, The Tokyo Electric Power Co. Inc., Yokohama 230-8510, Japan*

^b *Nippon Nuclear Fuel Development Co. Ltd., Japan*

^c *Applied Metallurgy and Chemistry Department, Toshiba Corporation, Japan*

^d *Nuclear Energy Equipment Manufacturing Department, Toshiba Corporation, Japan*

^e *Hitachi Works, Hitachi Ltd., Japan*

^f *Hitachi Research Laboratory, Hitachi Ltd., Japan*

Received 22 March 1997; accepted 10 August 1998

Abstract

Degradation of weldability in neutron irradiated austenitic stainless steel is an important issue to be addressed in the planning of proactive maintenance of light water reactor core internals. In this work, samples selected from reactor internal components which had been irradiated to fluence from 8.5×10^{22} to 1.4×10^{26} n/m² ($E > 1$ MeV) corresponding to helium content from 0.11 to 103 appm, respectively, were subjected to tungsten inert gas arc (TIG) welding with heat input ranged 0.6–16 kJ/cm. The weld defects were characterized by penetrant test and cross-sectional metallography. The integrity of the weld was better when there were less helium and at lower heat input. Tensile properties of weld joint containing 0.6 appm of helium fulfilled the requirement for unirradiated base metal. Repeated thermal cycles were found to be very hazardous. The results showed the combination of material helium content and weld heat input where materials can be welded with little concern to invite cracking. Also, the importance of using properly selected welding procedures to minimize thermal cycling was recognized. © 1999 Elsevier Science B.V. All rights reserved.

PACS: 25.55; 81.20.V; 61.80; 28.41.Q

1. Introduction

Austenitic stainless steel is the main constituent material used in the reactor internal structure of boiling water reactors (BWRs). It contains nickel as a major alloying element and boron as a trace element. Both these elements have a large cross-section to nuclear transmutation reaction by thermal neutrons, which results in helium production. The mobility of helium atoms in the austenite matrix is negligibly small within the temperature range of BWR operation, nominally around 560 K, hence BWRs have not incurred any detrimental effects from helium.

However, in the event of needed repair of irradiated stainless steel components, the helium effect is an important issue to be addressed. Since helium atoms will migrate to grain boundaries at elevated temperatures during welding, the strength of the grain boundaries is likely to be degraded resulting in intergranular cracking in the heat affected zone (HAZ). The susceptibility to weld cracking, however, is not simply dependent on the helium content. An attempt has been reported [1] to weld repair a cracked stainless steel tank (12.7 mm in thickness) of a military reactor. This repair was unsuccessful because of helium induced weld cracking [2] although the helium content was as low as 0.85 atomic parts per million of helium (appmHe) [3]. In another case, 1.0-mm thin plates obtained from the fast-reactor fuel component containing a maximum 30 appmHe were butt welded. No failure was found even in the bend test

* Corresponding author. Tel.: +81-45 585 8640; fax: +81-45 585 8647; e-mail: t0707232@pmail.tepco.co.jp.

[4]. These results suggest that the susceptibility to weld cracking is also dependent on other factors such as heat input, specimen dimensions and the intensity of restraint.

Subsequent efforts were made to minimize cracking using either neutron-irradiated steel or helium charged material. The use of special welding processes such as a low-penetration gas metal arc weld overlay technique [5] or a stress-modified welding technique [6] were shown to be favorable. Although use of these techniques may promise better repair welding, they are not readily applicable in actual cases, especially deep in water with limited access. In this work, a conventional tungsten inert gas arc (TIG) welding technique was selected and its applicability to neutron-irradiated austenitic stainless steels was examined considering the dependence on weld heat input of weld cracking susceptibility.

2. Materials and their helium contents

The samples tested are listed in Fig. 1 in increasing order of helium content. Types A and B samples were obtained from type 316L stainless steel (SUS316L) tube. Types C and E samples were obtained from type 304 stainless steel (SUS304) tube. Type D samples were cut from SUS304 plates. The chemical composition of each

sample was within the specification of Japan Industrial Standard (JIS) as given in Table 1. There were no data for boron content. All the samples were solution-annealed before irradiation. The nominal temperature of irradiation was 561 K. The samples were in contact with flowing high temperature water during irradiation so that the effect of gamma heating was considered to be small.

Helium contents in the sample varied over three orders of magnitude ranging 0.115–103 appmHe. The helium contents were obtained using the procedure given in Ref. [7] where number of thermally released ^4He atoms were counted by mass spectroscopy. Small pieces of samples for helium measurements were taken from locations where the effect of helium diffusion during welding and/or sampling could be neglected. The helium contents indicated in parentheses are interpolated values.

3. Welding procedures

In the present work, flat-position TIG welding was employed. In case of welding tubular samples, types A, B, C and E, one end was chucked and the sample was rotated under the welding torch. In case of welding plate samples, type D, the sample was fixed to a welding jig and the welding torch traveled along the longitudinal

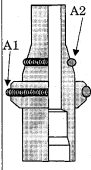
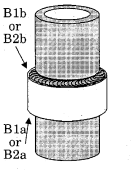

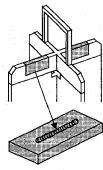

Sample type	Type A		Type B				Type C			Type D					Type E		
Number of sample	1		2				3			5					2		
Weld ID	A1	A2	B1a	B1b	B2a	B2b	C1	C2	C3	D1	D2	D3	D4	D5	E1	E2	
Material Specification	SUS316L		SUS316L				SUS304			SUS304					SUS304		
Dimensions	Outer diam.	39.0	22.2	17.3(tube)/23.5(collar)			16.0			length: 60, width: 30					17.3		
(mm)	Thickness	13.2	4.8	2.3(tube) + 3.0(collar)			1.5			8.0					2.3		
Helium content (appm)	0.115	0.217	(0.36)		(1.9)		(0.6)	4.98		3.98		8.30			103		
Fast fluence(n/m ² , E>1MeV)	~8.5×10 ²²		4×10 ²³		2.3×10 ²⁴		7×10 ²³		5×10 ²⁴		9×10 ²⁴		1.4×10 ²⁵			1.4×10 ²⁶	
Thermal fluence(n/m ²)	~4.5×10 ²³		—		—		—		1×10 ²⁵		9×10 ²⁴		1.3×10 ²⁵			1.6×10 ²⁶	
Heat input (kJ/cm)	7.68	7.51	2.46	2.70	2.57	2.55	1.20	0.58	1.26	7.1	5.3	7.1	10.8	16.4	1.05	1.88	
Appearance and position of welding																	

Fig. 1. Summary of the experimental conditions; materials specification, dimensions of the sample, neutron irradiation condition and content of helium generated and welding conditions. The drawings indicate the position of the bead. Helium contents in parentheses are interpolated values. The collars in type B samples were made of unirradiated SUS316L.

Table 1

Specification for chemical composition in weight per cent of tested material as defined in Japan Industrial Standard (JIS)

	C	Si	Mn	P	S	Ni	Cr	Mo	Fe
SUS304	<0.08	<1.00	<2.00	<0.045	<0.030	8.00 ~ 10.50	18.00 ~ 20.00	—	Balance
SUS316L	<0.030	<1.00	<2.00	<0.045	<0.030	12.00 ~ 15.00	16.00 ~ 18.00	2.00 ~ 3.00	Balance

centerline of the sample. Simulated filler material was used when necessary since the welding torch used did not have a filler metal supplying capability. No groove was prepared on irradiated samples.

For type A sample, two single-pass circumferential welds, A1 and A2 were made on an identical sample as depicted in Fig. 1. Simulated filler metal (2 mm^w–1.6 mm^t) made of SUS316L was tack welded to the flange rim prior to A1 welding. A nominal heat input of 7.68 kJ/cm could melt all of this filler. Weld A2 was made where the helium content was twice that of A1. A2 was welded without filler metal with a 7.51 kJ/cm heat input.

For type B sample, two samples of 60 mm in length, B1 and B2, were obtained from an identical tube. The location where B2 was obtained was a little closer to the reactor core than where B1 was obtained. The estimated neutron fluence and helium content for B2 were therefore larger than those for B1. Two ‘collars’ made of unirradiated SUS316L were prepared. The collar was 3 mm in thickness except at both ends that were thinned to 1.5 mm for the purpose of simulating filler metal. The collar was tack welded to the irradiated tube sample and then both ends were welded with heat input about 2.5 kJ/cm.

For type C sample, three samples of 90 mm in length, C1, C2 and C3 were selected. The neutron fluence, helium content and weld heat input is shown in Fig. 1. Each sample was rotated 400° to overlap the start and the end of the bead. No filler metal was applied. C2 was welded with low heat input and was a half-wall-thickness weld. Welded joint tensile test specimens were cut out from the quadrantal tube section of the through-wall-welded C1 and C3. The dimension of the gauge section was 3 mm^w–1.5 mm^t–20 mm^l. Another quadrant was subjected to the surface-bending test using a fixture that had a plunger with a 3 mm radius of curvature.

Type D samples were 8 mm thick plates; high weld heat input could be applied without melt down. Welding was carried out in a chamber set two meters under water to minimize personal exposure. The bead-on-plate test was done with four levels of nominal heat input: 5, 7, 11 and 16 kJ/cm. The entire bead including both the starting point and the crater treated terminating point were on the sample; no run-on, run-off tab was used.

Type E samples were the most heavily irradiated tubular material and two samples of 90 mm in length, E1 and E2, were used. E1 welded with 1.05 kJ/cm heat input was a half-wall-thickness weld. E2 welded with 1.88 kJ/cm heat input was a through-wall-thickness weld. Sample was welded by rotating it 435° to ensure the overlapping of start and end of the bead.

After the welding, cracking was inspected by liquid penetrant testing (PT). For types A, B, C and E samples, only outer surface was inspected by visible dye PT. Type

D samples were inspected by fluorescence PT in an underwater chamber. Selected samples, mainly PT sound welds, were further examined by cross-sectional metallography.

4. Test results

4.1. Type A sample

The welded surface was examined by PT and no cracks were detected either on A1 or on A2. The absence of cracks in both welds was also confirmed by cross-sectional metallography.

4.2. Type B samples

The appearance of B2 is shown in Fig. 2(a). No defects were detected both by visual observation and by PT. Cross-sectional metallographs of B1b are shown in Fig. 2(b) and (c). Dispersed black dots and dots in rows were observed in the as-polished cross-section (Fig. 2(b)); these dots were dispersed in the weld metal and aligned along the grain boundaries in the HAZ, respectively. Grain boundaries decorated with these black dots were more severely etched by oxalic acid test (Fig. 2(c)). This change was observed only in irradiated material, not in the unirradiated collar, and was supposed to be a result of the helium effects.

4.3. Type C samples

No defects were detected by outer surface PT in all welds, C1, C2 and C3. However, cross-sectional observation of C3 (5×10^{24} n/m², 1.26 kJ/cm, through-wall-thickness welding) revealed the presence of cracks in the HAZ of inner surface. In the case of C1 (7×10^{23} n/m², 1.2 kJ/cm, through-wall), no cracks were found, but grain boundaries in the HAZ near the inner surface were modified with helium bubbles like those observed in Fig. 2(b). In the case of C2 (5×10^{24} n/m², 0.58 kJ/cm, half-wall-thickness welding), no defects were identified by metallography.

Figs. 3 and 4 show the weld joint tensile test results taken from C1 and C3. The strain in Fig. 3 was defined as the cross-head displacement divided by the gauge length, 20 mm.

C1 (7×10^{23} n/m²) showed almost the same strength and elongation as unirradiated materials; both the ultimate strength and total elongation exceeded the JIS requirement. The appearance and fractograph of fractured specimens are shown in Fig. 4(a)–(c). The deformation was extended to the entire gauge area including weld metal, HAZ and base metal. The fracture surface con-

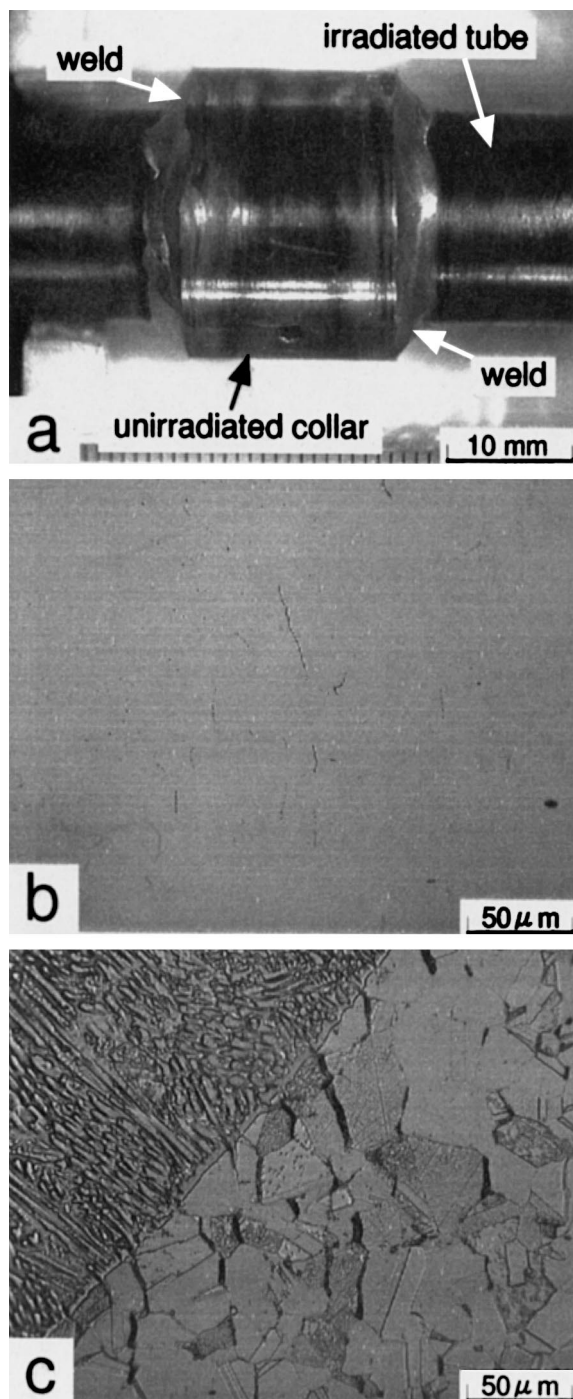


Fig. 2. (a) The appearance of welded B2 sample with 1.9 appmHe. The cross-section of weld B1b containing 0.36 appmHe (b) before and (c) after etching indicated the formation of aligned bubbles on grain boundaries.

sisted of the transgranular (TG) ductile dimple fracture region (marked D in the sketch) and intergranular (IG) fracture region (marked D+IG in the sketch). The latter

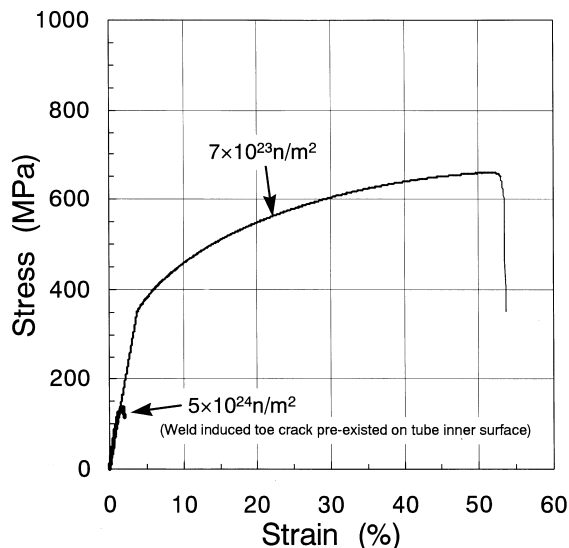


Fig. 3. The stress-strain curves for tensile specimens cut from weld C1 (He = 0.6 appm) and weld C3 (He = 5 appm).

region was, however, covered with elongated IG dimples as shown in Fig. 4(c). This indicated that no cracks were introduced by welding alone, and that enough ductility remained throughout the cross-section.

In contrast to C1, C3 ($5 \times 10^{24} \text{ n/m}^2$) fractured with the slightest ductility. The major part, 87%, of the fractured surface was covered with IG facets that were all decorated by dimples as shown in Fig. 4(f). These dimples were smooth, unlike the elongated ones in C1 (Fig. 4(c)). This indicated that the IG fractured region corresponded to the extent of weld cracking before tensile loading. The remainder of the fracture surface, 13%, was covered with TG ductile dimples.

Fig. 5 shows an example of surface-bending-test result for the specimen cut from C3. Although this tubular specimen contained a deep inner surface HAZ crack, the outer surface, which was tensile-strained, was free of PT indication. Specimen from C1 was also free of PT indication.

4.4. Type D samples

The test results are summarized in Fig. 6. The tested conditions in which there was no PT indication were: lower fluence sample ($9 \times 10^{24} \text{ n/m}^2$) welded at 7.1 kJ/cm (D1), and higher fluence samples ($1.4 \times 10^{25} \text{ n/m}^2$) welded at 5.3 or 7.1 kJ/cm (D2 and D3). When the higher fluence samples were welded at higher heat input, 10.8 or 16.4 kJ/cm (D4 and D5), PT indication appeared in parallel to the welding direction in the HAZ. Cross-sectional examinations were made on selected sound welds. Fig. 7 is an example for D3. Pores in the weld metal were considered to be formed from the helium

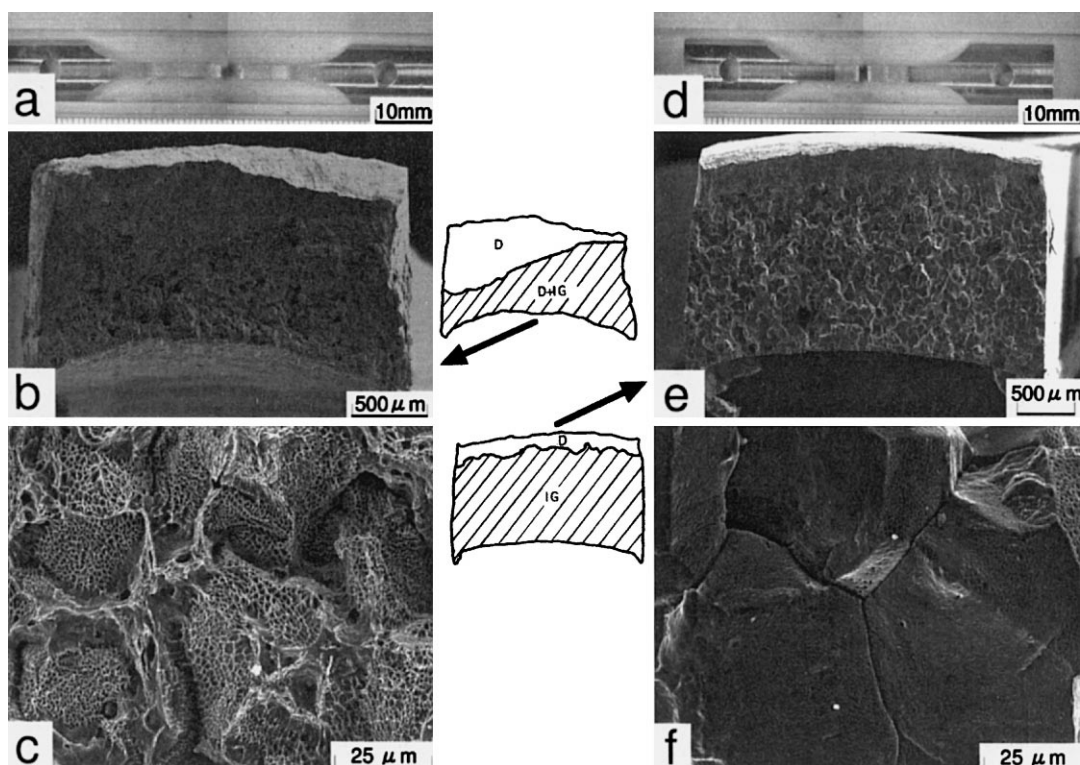


Fig. 4. The appearance (a, d), the whole cross-section (b, e) and magnified view of intergranularly fractured surface (c, f) for tensile-tested weld C1 (a, b, c) and weld C3 (d, e, f). The difference in the mode of intergranular fracture was apparent in (c) which was covered with ductile dimples and in (f) which was covered with smooth dimples. The inserted sketches represent (b) and (e) indicating the mode of fracture: D for ductile dimple fracture, D + IG for intergranular fracture with ductile dimples as shown in (c), IG for intergranular fracture.

atoms held in solution in the metal matrix before welding. No cracking was observed either in the HAZ or in the weld metal when the cross-section was obtained from the middle of the weld line (Fig. 7(a)). Obvious cracking appeared, however, in the cross-section obtained from the crater treated position (Fig. 7(b)). These features occurred in other examined welds: more severe cracking was found in the crater area while little cracking could be found in the middle of the weld line.

4.5. Type E samples

No PT indication was detected in E1. In E2, one was detected but only in the overlapped part of the weld bead. The remainder of the circumference, i.e. the middle of the E2, was free of PT indication. Fig. 8(a) shows an example of the cross-section from this part. The presence of many pores in the weld metal reflected the high helium concentration (>100 appmHe) of this material. Note that small cracks were found on the inner surface but not on the outer surface. Fig. 8(b) and (c) are magnified views of the weld toe area of the outer and inner surfaces, respectively. The inner surface crack ran

along grain boundaries in the HAZ. The HAZ of the outer surface toe contained no cracks, but the grain boundaries were modified by aligned bubbles. This was similar to the features seen in Fig. 2(b).

5. Discussion

The weldability test results are summarized in Fig. 9 where the extent of cracking or produced defects observed in the weldment are categorized with five different symbols. It is clear that the integrity of the weld was better in lower helium content material and at lower heat input. Cracking became more severe as helium content became higher and/or heat input became larger. This trend is well understood by the helium embrittlement mechanism. By increasing the heat input, the width of the HAZ becomes wider where the temperature is raised high enough to make helium atoms mobile in the metal matrix. Also, the volume of weld metal becomes larger resulting in larger solidification shrinkage thus generating higher level of tensile stress in the HAZ. The presence of tensile stress is known to promote helium

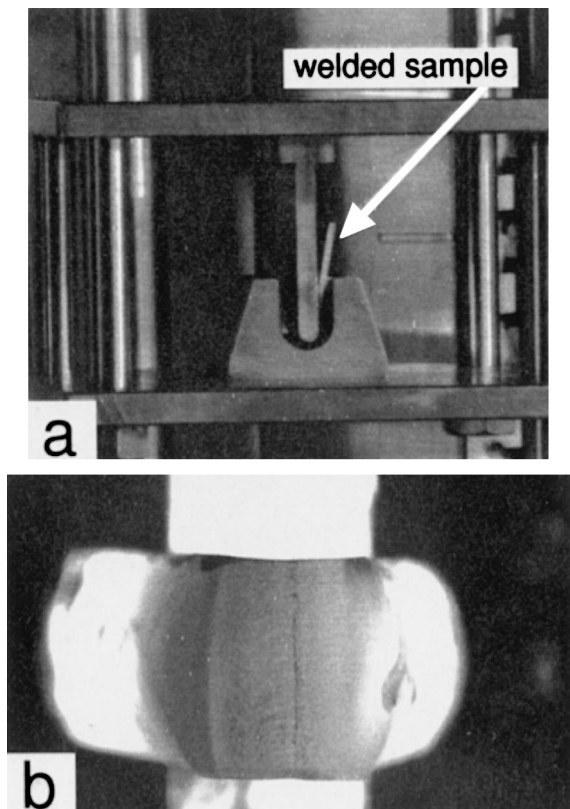


Fig. 5. The test fixture (a) used for the surface-bending-test on specimens from weld C1 and C3. (b) The bent surface of the specimen from weld C3 (He = 5 appm) was free of defects by dye penetrant test.

migration to the grain boundaries (GBs) and enhance the nucleation and growth of helium bubbles therein [8]. These effects, along with the higher content of helium, lead to more severe cracking. Therefore, reduced heat input would be very beneficial to improve weld quality. Use of a high energy density heat source, such as laser or electron beam, can minimize the heat input to the material thus reducing the temperature elevation and thermal stress and making the cooling rate in the HAZ larger. These effects will help suppress the diffusion of helium to GBs and make the weld cracking less likely.

5.1. Mechanical properties of the weld

The cross-section of C1, where helium bubbles on GBs were observed, showed that the helium atoms have had aggregated on GBs during welding. The tensile and bending properties were, however, not degraded compared to those for unirradiated materials (Fig. 3). The elongated nature of the IG dimples observed in microfractograph (Fig. 4(c)) indicated that the ductility of the

GB was little affected despite the GB helium bubble formation.

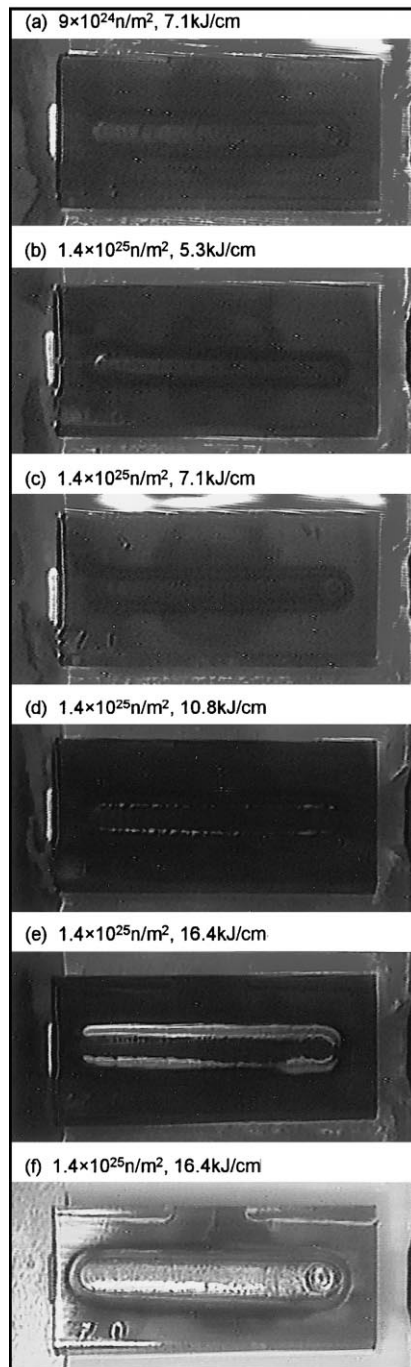


Fig. 6. The weld test results on type D samples. Fluorescent penetrant test was used to detect surface cracking. No surface cracking was observed in (a), (b) and (c). Bright indications near the toe of the bead were found in (d) and (e) which corresponded to cracks. (f) shows the appearance of the weld bead.

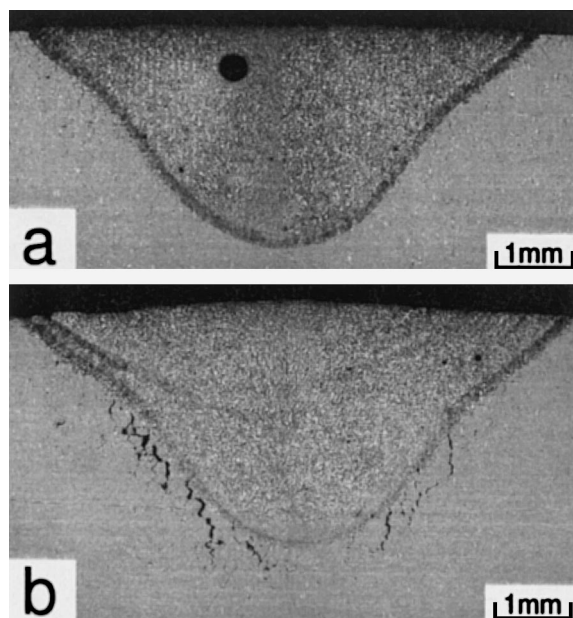


Fig. 7. The cross-sectional metallography of weld D3 (He = 8.3 appm) welded at 7.1 kJ/cm. The cross-section in (a) obtained from the middle of the bead contained no cracking while that in (b) obtained from the crater treated position contained sub-surface cracking.

The tensile test on C3, containing 5 appmHe, provided another insight. The nominal tensile strength of this weld was 137 MPa and the nominal total elongation was 1.98% over a 20 mm gauge length including the joint itself; these nominal values fell short of the requirement. However, it must be considered that the area that survived cracking during welding was very limited. If only the area indicated by D in Fig. 4(e), 13% of the initial cross-section, was subjected to the tensile load of 617 N ($= 137 \text{ MPa} \times 3 \text{ mm}^2 \times 1.5 \times \text{mm}^2$), the net stress in this area exceeds 1 GPa; this value is larger than the tensile strength of this material which is around 750 MPa before welding. So, it can be inferred that at least the uncracked part of the fracture surface had equivalent tensile strength to those of unwelded material. This inference was also confirmed by other observations: the mode of fracture in this part was TG with ductile dimples with no discernible effect of helium embrittlement; no defect was introduced in this part by bending test even the estimated strain exceeded 20%. The tensile deformation in C3 was also limited to the vicinity of the pre-existed crack. So the local ductility of the uncracked part can be considered to be high enough judging from the ductile manner of the fracture.

Metallography of these two welds revealed the presence of aligned helium bubbles on GBs in the HAZ. This change is evidence of a potential effect of helium embrittlement, however, it can reasonably be

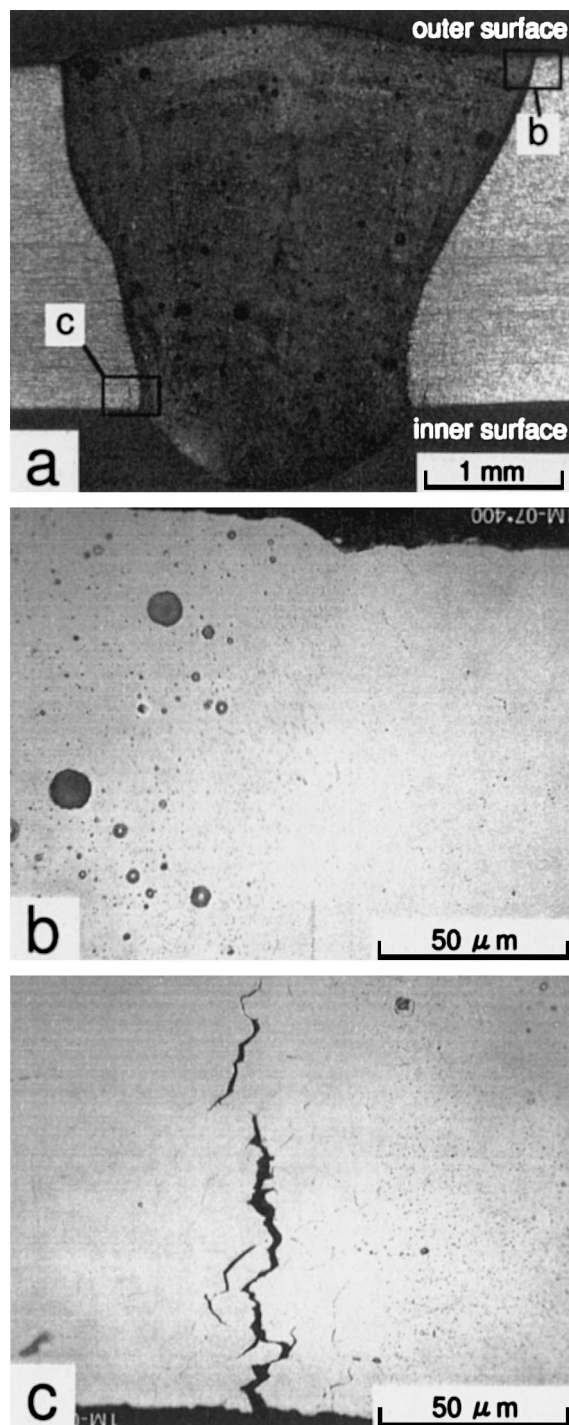


Fig. 8. (a) The cross-section at the middle of the circumferential weld on sample E2 (He = 103 appm). Detailed observation near the weld toe showed the absence of crack on the outer surface (b) and cracking on the inner surface (c).

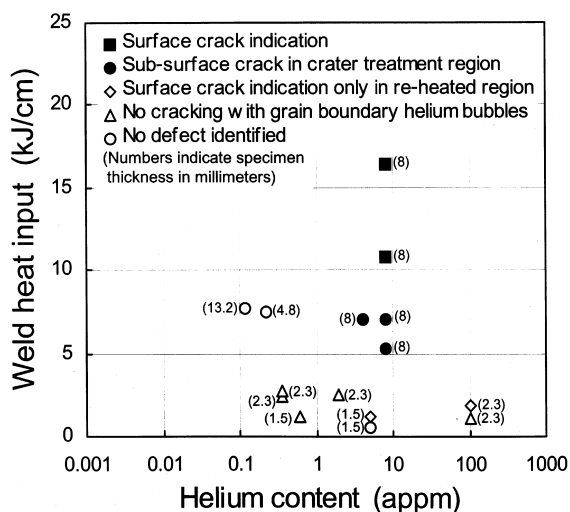


Fig. 9. The dependence of the character of weld-induced defects on helium content and weld heat input.

inferred as not to be detrimental to the strength of the welded joint.

5.2. Cracking incurring conditions

In this work, the distribution of cracks, if present, was not uniform along the weld bead. If a combined condition of helium content and welding heat input was judged to be sound, it does not mean that the total of the weld line was thoroughly defect free. Two types of conditions that incur cracking were identified from this investigation: the overlap of the weld bead in tubular samples (E2, inner surface of C3); and the crater treatment region at termination of a stringer bead (Fig. 7(b)). When a closed weld line must be constituted, like a circumferential welding on tubes, there is always an overlap of the bead, at least at the end of welding. In this overlap region, the first welding cycle will alter the state of presence of helium atoms in the HAZ somehow to increase the cracking susceptibility. The second heat cycle thereon will further enhance the helium inflow to HAZ GB and this will make IG cracking more easily upon cooling. In the crater treatment region, the welding current is gradually diminished with the torch woven. The HAZ around the crater will therefore experience repeated heat cycles during cooling. This cycling is evident from the weld metal microstructure in Fig. 7(b); and just beneath the crater, severe cracking was observed even though there was no PT-detectable surface cracking in this weld bead. From these observations, a conclusion can be drawn that those positions that experienced repeated welding heat cycles were liable to crack. This suggests the importance of proper design of the weldment and choice of the welding procedure. Such

welding techniques as multilayer welding or overlay welding which require bead overlap, or welding which requires elaborate crater treatment should be minimized to achieve defect-free welding.

Another position where cracking was often found was weld toe at the inner surface of circumferential weld of tubular samples such as in C3 (Fig. 4(e)) and E2 (Fig. 8). When such circumferential weld is placed on tubes or pipes, it is well known that there will be a tensile residual stress on inner surface and a compressive residual stress on outer surface. Hence, the formation of inner surface cracking can be attributed to the enhanced helium aggregation to GBs, which is in agreement with the mechanism proposed in Ref. [8]. In E1 and E2, no outer surface crack was observed, except at re-heated region in E2, despite their very high helium content (103 appmHe). The generation of compressive residual stress on outer surface upon cooling could have suppressed the formation of cracks. Those regions beneath the outer surface were free from IG fracture in tensile test as noted in the previous section. These results are also in good agreement with that in Ref. [6] where the possibility to suppress cracking is discussed by applying a compressive stress normal to the welding direction during welding.

5.3. Helium content in the material

Austenitic stainless steels contain nickel and a trace of boron. Nuclear transmutation reaction of these elements produce helium atoms via $^{58}\text{Ni}(n, \gamma)^{59}\text{Ni}(n, \alpha)^{56}\text{Fe}$ and $^{10}\text{B}(n, \alpha)^7\text{Li}$. Helium from nickel is produced by a two-step reaction, thus the amount of product is proportional to the square of the thermal neutron fluence. Helium production from boron is in proportion to the thermal neutron fluence, until the burn-up of boron is negligible. The concentration of

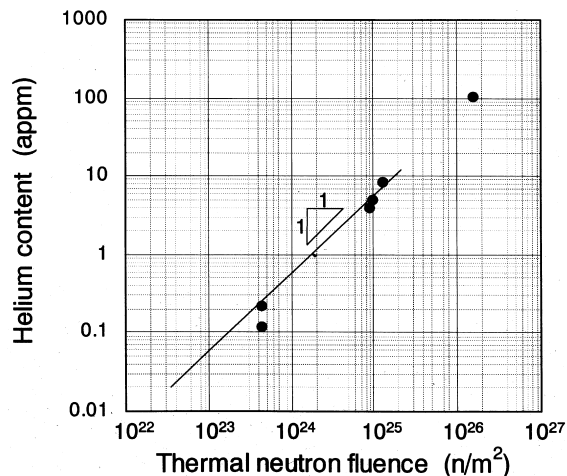


Fig. 10. The dependence of helium content on thermal neutron fluence.

helium is therefore dominated by impurity boron content in low fluence region, while the contribution from nickel increases in higher fluence region. Fig. 10 shows the relation between helium content and thermal neutron fluence, where only the helium content value actually analyzed are shown, and those in parentheses in Fig. 1 are not included. A good one-to-one correspondence between helium content and thermal fluence can be seen for a wide range of irradiation levels as shown in the figure. The gradient of the line in the figure is unity, which suggests that the dominating contributor to helium production was boron in most of this fluence range. The highest helium content of 103 appmHe was, however, unrealistic by considering the contribution from boron alone: the impurity level of boron is usually much lower. Since the trace boron is supposed to have burnt-up in this fluence, the contribution from the transmutation of nickel should be incorporated.

6. Summary

1. Weldability tests by TIG welding procedure were performed for austenitic stainless steels neutron-irradiated in power reactors to fluence from 8.5×10^{22} to 1.4×10^{26} n/m² ($E > 1$ MeV) corresponding to helium content from 0.11 to 103 appm, respectively.
2. The integrity of the welded joint was better in lower helium content material and with smaller weld heat input. Unirradiated steel was successfully welded to the irradiated steel containing 1.9 appmHe. The mechanical properties of the welded-joint containing 0.6 appmHe satisfied the JIS requirement for unirradiated base metal. No defect was formed in the sample containing 0.1 appmHe after welding at 7 kJ/cm heat input with filler metal deposition.
3. The severity of the helium effects induced by welding varied from severe surface cracking, to subsurface cracking, and to helium bubble formation along grain boundaries as helium content became smaller.
4. The mechanical property of the weld was not affected by the presence of helium atoms if they only form grain boundary bubbles and no longer grow into cracks upon welding.
5. A fully ductile fracture surface was obtained by tensile test of the welded type 304 tube with 5 appmHe

although the remainder of the cross-section cracked before the tensile test.

6. Weld-induced cracks were often found under the crater treatment and at the bead overlap where the material experienced repeated heat cycles. This observation suggested the importance of proper design of welding procedures to avoid these crack-inviting conditions.

Acknowledgements

The co-sponsorship to this work by other boiling water reactor owners of Japan, Tohoku Electric Power Co. Inc., Chubu Electric Power Co. Inc., Hokuriku Electric Power Co. Inc., The Chugoku Electric Power Co. Inc. and The Japan Atomic Power Company is gratefully acknowledged.

References

- [1] J.P. Maloney, D. Baker, W.R. Kennedy, W.A. Day, J.B. McClain, W.G. Fraser, D.H. McKenney, H.R. Huxford, C.A. Meyer, K.E. Kehr, R.F. Mittelberg, J.E. Walls, Repair of a Nuclear Reactor Vessel, AEC R&D report, Savannah River Laboratory, DP-1199, 1969.
- [2] A.K. Birchenall, presented in TMS-AIME symposium on Welding of Helium-Containing Metals, Indianapolis, IN, USA, October 3, 1989, DP-MS-89-41.
- [3] W.R. Kanne Jr., G.T. Chandler, D.Z. Nelson, E.A. Franco-Ferreira, *J. Nucl. Mater.* 225 (1995) 69.
- [4] S.D. Atkin, ADIP Quarterly progress report, DOE/ER-0045/7, 1981, p. 110.
- [5] W.R. Kanne Jr., G.J. Bruck, A. Madeyski, D.A. Lohmeier, M.R. Louthan Jr., D.T. Rankin, R.P. Shogan, G.G. Lessmann, E.A. Franco-Ferreira, in: Proc. 5th Int. Symp. on Environmental Degradation of Materials in Nuclear Power Systems – Water Reactors, Monterey, CA, August 1991, The American Nuclear Society, p. 390.
- [6] C.A. Wang, M.L. Grossbeck, B.A. Chin, in: A.S. Kumar, D.S. Gelles, R.K. Nanstad, E.A. Little (Eds.), *Effects of Radiation on Materials: 16th Int. Symp.*, ASTM STP 1175, ASTM, PA, 1994, p. 779.
- [7] H. Farrar, B.M. Oliver, *J. Vac. Sci. Tech. A* 4 (1986) 1740.
- [8] H.T. Lin, M.L. Grossbeck, B.A. Chin, *Metal. Trans. A*, V21A (1990) 2585.